Journal of Materials Research and Technology 29 (2024) 3228–3236

Contents lists available at ScienceDirect

Journal of Materials Research and Technology

journal homepage: www.elsevier.com/locate/jmrt

Structural and mechanical optimization of porous alumina structures fabricated by carbon sacrificial template

Manuela González-Sánchez, Pedro Rivero-Antúnez, Francisco Luis Cumbrera-Hernández, Víctor Morales-Flórez *

Departamento de Física de la Materia Condensada, Universidad de Sevilla, Sevilla 41012, Spain

ARTICLE INFO

Keywords:
Porous alumina (Al_2O_3)
Carbon sacrificial template
Mechanical properties
Reactive spark plasma sintering
Taguchi method

ABSTRACT

The Taguchi method is used to optimize the manufacture of porous alumina made through reactive spark plasma sintering and carbon sacrificial template. The goal is to design a new versatile procedure that allows the fabrication of porous alumina with tailored physical properties. The structural and mechanical properties taken as target parameters were the subtle combination of porosity and Young's modulus of the human cortical bone: typical pore size >100 μm, and Young's modulus in the range of 3–30 GPa. The input factors of the Taguchi method are wt.% of carbon, sintering time, calcination heating rate, and final heat treatment. Hg porosimetry, electron microscopy, uniaxial compression and computer aided tomography were used for the characterization of the porosity, pore size distribution, pore interconnectivity, and Young's modulus. Finally, according to the conclusions of the Taguchi analysis, the parameters of the process were changed for the fabrication of the new samples with optimized properties. Highly porous structures with 90% interconnectivity, Young modulus of 5.5 ± 1.1 GPa, and compression strength of 49 ± 20 MPa, were obtained, successfully emulating the targeted properties.

1. Introduction

Alumina (Al_2O_3) is an advanced ceramic material due to some excellent properties: high hardness, chemically inert, refractory and low thermal and electrical conductivities. These characteristics allow its use in very different industries, such as tool making, insulating, or electronics [1,2]. In addition, porous alumina has specific applications, such as membranes, electric substrates [3], or even biomedical applications due to its biocompatibility [4,5]. Hence, much research has been devoted to the design of procedures for the fabrication of porous alumina [3,6] and the relations between its structural properties, such as its microstructure, porosity and pore size, and its mechanical properties have been widely studied [7].

In particular, the reduction of the Young's modulus of alumina with increasing porosity opens the possibility of tuning the mechanical properties of alumina just by adjusting its porosity. This strategy clears the road for designing alumina-based constructs for specific applications that require a particular combination of properties. A suggestive example is the human cortical bone, which exhibits a subtle relation between porosity (interconnected pores with sizes > 100 μm) [8,9] and mechanical properties (e.g., Young's modulus between 3 and 30 GPa) [10]. It is worth recalling that a mechanical mismatch between an implant and the targeted cortical bone leads to problems such as stress shielding, especially severe on cortical bone with high mechanical solicitations, and most of the materials used for bone implants, such as metallic and 3D biodegradable scaffolds, typically exhibit enormous differences between their mechanical properties and those of the bone [11–18]. This work tackles the challenge of designing a specific and versatile procedure for the fabrication of porous alumina taking advantage of the known reduction of the mechanical properties with increasing porosity, and, more precisely, to obtain alumina-based porous constructs with a controlled combination of specific porosity and mechanical properties. In particular, the combination of structural and mechanical properties of the human cortical bone have been selected as the target properties. This research, jointly with other investigations aiming at the bioactivation of ceramic materials [19–21], could enable new possibilities for alumina-based materials for biostructural applications, which may display higher mechanical properties than typical calcium phosphate bioceramics such as TCP or HA.

To achieve this goal, this work considers a procedure based on the strategy of carbon sacrificial template this work considers a procedure based on the strategy of sacrificial template, which has been already employed for the preparation of porous alumina, using as

* Correspondence to: Department of Condensed-Matter Physics, University of Seville, P.O. 1065, Seville 41080, Spain.
E-mail address: vmorales@us.es (V. Morales-Flórez).
URL: http://grupo.us.es/fqm393/ (V. Morales-Flórez).

https://doi.org/10.1016/j.jmrt.2024.02.099
Received 3 November 2023; Accepted 12 February 2024
Available online 14 February 2024

template different phases, such as polymer spheres [22], rice husk and sugarcane bagasse [23], starch [24], cellulose [25], or carbonaceous phases [22,26–30]. Thus, finding the best set of parameters affecting the fabrication process, such as the amount and the particle size of the sacrificial carbon, the sintering pressure, the heating ramps, the sintering and calcination temperatures, and thermal consolidation conditions, among others, has been the subject of study of this research. In this regard, the Design Of Experiments (DOE) is a useful tool for providing knowledge about the influence of each factor and about possible interactions. Actually, it avoids blind trial and error experiments and helps to optimize the search for the appropriate values of the parameters involved in a manufacturing process because resources (such as time and materials) are limited, and many experiments cannot be performed [31]. DOE includes advanced statistical tools such as the Full Factorial and Fractional Factorial methods. An unbiased Fractional method is the Taguchi analysis [32], which is nowadays the best way to find the minimum number of experiments to be performed to optimize a complex process. It has typically been used in industrial processes such as the production of sugar [33], biotechnological applications [34], fabrication of hydroxyapatite–alumina–titanium nanocomposites [35] and artificial bone grafts [36,37].

The deep foundations of the Taguchi method rely in the concept of *Loss of Quality*. According to Taguchi's philosophy, loss continually increases as the product deviates from the target value. Hence, the quadratic *Loss function* is expressed as:

$$L = K(Y - T)^2 \tag{1}$$

where L is the *Loss*, K is a constant, T the target value and Y the measured value. By applying a logarithmic transformation to the above equation we obtain a measure of robustness: the signal-to-noise ratio, S/N. In Taguchi designs, the S/N is used to identify control factors that reduce variability in a process by minimizing the effects of uncontrollable factors (noise factors). Then, the signal-to-noise ratio is calculated for each factor level combination. According to the "the larger is better" criterion, the formula of the S/N ratio using base 10 log is:

$$S/N = -10 \cdot log(\sum(Y^2)/n). \tag{2}$$

This work is based in previous results that proved the successfull use of carbon phases as sacrificial template for the fabrication of porous alumina by SPS [30]. It was also shown the crucial role of the final heat treatment in order to consolidate the porous skeleton. In the current work, to avoid the typical trial-and-error methodology, the conscious optimization of the procedure has been undertaken through the DOE Taguchi method. In this case, the manufacturing process considers different precursor, the sol–gel method, and the reactive spark plasma sintering (rSPS) process [38]. Optimization pursues porous alumina constructs that exhibit specific physical properties. The resulting constructs are characterized to obtain their specific microstructural and mechanical properties. The analysis resulting from the Taguchi method gives the most significant set of parameters for the fabrication, and, finally, this set of parameters is considered for fabricating optimized samples.

2. Materials and methods

2.1. Taguchi's method for the fabrication of the samples

The Taguchi method has been used for the optimization of the fabrication process of the porous alumina structures. The fabrication started with a mixture of boehmite particles (γ-AOOH, from commercial sol NyacolNano Technologies, Inc., dispersed sizes = 60–90 nm, crystallite size = 15 nm) and α-Al_2O_3 seeds (2.0 wt% of the final alumina mass, from Nanostructured and Amorphous Materials, Inc., 99% purity, particle size = 30–40 nm). The addition of the seeds promotes direct phase change from boehmite to α-Al_2O_3, preventing the appearance of transition aluminas, such as γ-Al_2O_3, and the formation of vermicular structures. The boehmite sol and seeds were dispersed by vigorous stirring (15 min at 1000 rpm). This seeded sol was rapidly gelled by adding ammonia drops, and dried 48 h in a conventional stove at 60 °C. The resulting white xerogel was mortared and sieved to obtain a fine white powder. This procedure is described in detail and deeply discussed in [38]. These powders and the corresponding mass of carbon (charcoal activated for gas chromatography, Supelco-Merck, Darmstadt, Germany, purity: 92.5%, density: 2.160 g/cm^3, major impurities: Si, Al, S, Ca, and Fe, and a particle size of 490 ±130 μm) were manually mixed in an alumina mortar.

The input and output factors of the Taguchi method were selected based on the results of previous work [30], in which a first tentative of fabrication was introduced, but no systematic research of the design of the experimental procedure was performed. The number of factors and the range covered by the selected levels was decided according to our previous experience, and to have a reasonable number of quasi-experiments. Thus, among all the different parameters defining the procedure, five were selected as input factors to be analyzed, with two levels (values) each, while the rest were kept constant at standard values. Among all the physical properties of the obtained materials to be monitorized, five were selected as output factors.

Regarding the input factors, the amount of carbon is t he first one ("A") for the Taguchi method. According to the results of the aforementioned study, the necessary porosity for alumina samples to have a Young's modulus similar to that of the human cortical bone was established to be between 40% and 90%. So, aiming samples with porosities between 40% and 50%, 54 wt% and 64 wt% of sacrificial carbon should be considered, respectively, according to their densities, and assuming a perfect densification of the alumina skeleton. In this work, considering that perfect sintering of the skeleton will not occur, quite lower amounts of carbon were considered: 40 wt% and 50 wt%. The composite powder is mounted in a cylindrical graphite die, and sintered by reactive SPS (Dr. Sinter Lab Inc., model 515S, Kanagawa, Japan). The sintering of the powders was done at 1500 °C, with a heating rate of 100 °C/min under uniaxial pressure (75 MPa) and vacuum. During the heating ramp of the SPS, the phase change from boehmite to α-alumina occurs, avoiding intermediate alumina phases (such as γ-alumina), driven by the α-Al_2O_3 seeding [38,39]. The dwell time at the sintering temperature is the factor "B". Subsequently, the porosity is created by the calcination of the carbon. Hence, carbon was removed from the sintered sample by calcination in air in a muffle furnace (Carbolite Elf 11/6B, Hope Valley, England) at 900 °C for 5 h, where the heating rate is the factor "C". Finally, the resulting porous structures received a heat treatment to be consolidated in a tubular furnace (TERMOLAB – Fornos elétricos, Águeda, Portugal) at maximum temperature and dwell time under study (factors "D" and "E", respectively). The complete process is sketched in Fig. 1, where the selected values of the fixed parameters and those considered for the two-level factors of the Taguchi analysis are indicated.

An $L8(2^5)$ Taguchi arrangement was selected. Among all the 2^5 combinations of the two levels of each input factor (quasiexperiments), the Taguchi method selected the eight ones that were strictly necessary for revealing which are the most influential factors. Additionally, this method classifies the factors according to their relevance on the final outcome. In Table 1, all the details of the eight quasiexperiments are summarized. The sample series of each quasiexperiment was labeled as TX, where X is the number of the quasiexperiment.

The output factors are defined as follows: first, the target is to obtain porous structures with enough manageability (qualitative factor with three levels: 1 = poor, 2 = medium, and 3 = good); second, the total porosity has to be as high as possible; third, the typical pores have to be as large as possible; fourth, the existence of pores that favor bone regeneration and cell proliferation (>100 μm) has to be ensured (qualitative factor: 1 = no, 2 = yes); and finally, the Young's modulus has to be similar to that of cortical bone (3–30 GPa) [11,40,41]. The definition of the values of the output factors was established according to the "the larger is better" criterion, so, the maximum values of all the five output factors will be aimed.

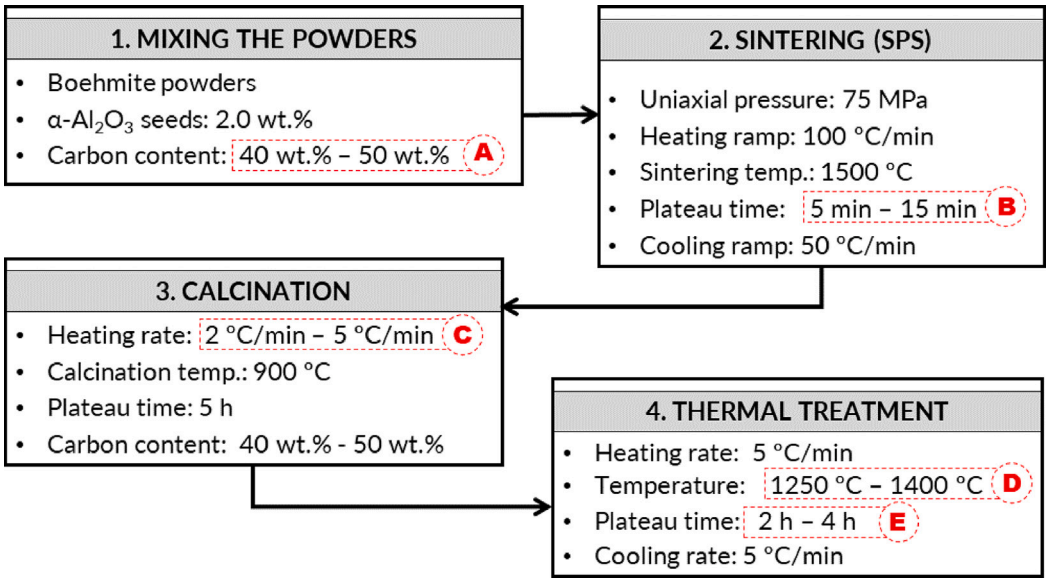

Fig. 1. Sketch of the fabrication procedure. The values of the fixed parameters of the process are indicated in the sketch. The five factors considered for Taguchi's analysis are framed in a red dashed box, indicating the values for the two levels considered, and labeled from *A* to *E*.

Table 1
Selected levels of each factor for the eight quasiexperiments proposed by the Taguchi method.

Taguchi factor	A	B	C	D	E
Quasiexperiment	Carbon content (wt.%)	SPS plateau (min)	Calcination heating ramp (°C/min)	Thermal treatment temp. (°C)	Thermal treatment plateau (h)
T1	40	5	2	1250	2
T2	40	5	2	1400	4
T3	40	15	5	1250	2
T4	40	15	5	1400	4
T5	50	5	5	1250	4
T6	50	5	5	1400	2
T7	50	15	2	1250	4
T8	50	15	2	1400	2

2.2. Characterization of the samples

All the porous samples obtained were weighted after the calcination and the heat treatment for consolidation. Chemical composition was estimated by X-ray fluorescence (XRF, AXIOS Panalytical, with an Rh tube). The density of the samples was measured assuming the density of bulk alumina (3.985 g/cm^3) for the density of the skeleton. The total porosity and the pore size distribution (PSD) were determined by Hg porosimetry (Quantrachrome Inc., model Poromaster 60GT) and the typical pore size was estimated as the pore size corresponding to the maximum specific pore volume. Further structural analyses were made by Scanning Electron Microscopy (SEM) with an FEI (model Teneo) working with an acceleration voltage of 2 kV, and Computer Aided Tomography (CAT) with a Zeiss Versa tomograph (model Xradia 610), using a voltage and current of 50 kV and 89.9 μA, respectively, and a voxel side size of 2.7184 μm. The total porous volume and the interconnectivity of the porosity were estimated from the study of the porous space with the help of the ImageJ and AVIZO software tools for the analysis of CAT images. The interconnectivity was assessed as the percentage of pore volume that belongs to the largest element of the pore space. The mechanical characterization was made through uniaxial compression tests in an Instron model 580, using a 5 kN load cell and deformation rate of 0.5 mm/min, and using the Bluehill INSTRON software for the analysis of the stress–strain curves. For these tests, 6 mm *x* 3 mm *x* 3 mm parallelepipeds were cut, in accordance with the ASTM standard 7012-04. The load axis of the uniaxial compression tests was perpendicular to the load applied during sintering. The Young's moduli were calculated by taking the average of the slopes determined by the linear fit of the stress–strain curves of each series of samples. The values of the compression strength were also estimated from the average of the maximum loads borne by the samples. Five samples were considered for the statistics, and the standard deviations of the data series were considered as uncertainties.

3. Results and discussion

Firstly, the removal of the sacrificial template was assessed by weighing the samples throughout the process. It was confirmed that, typically, the weight loss due to the calcination corresponded to 88% of the total mass of carbon sacrificial template. So a 12% of the mass of the sacrificial template remained after calcination, including the impurities (Si, Al, S, Ca, and Fe, as revealed by XRF, which are not removed under these conditions) and very small amounts of carbon that diffused within the alumina skeleton. In addition, the samples from the different quasiexperiments proposed by the Taguchi method were checked to verify their manageability, and next they were tested to obtain the porosity and Young's modulus. The results are presented in Table 2; they are the outputs that were used for the Taguchi analysis. Regarding the first output factor, manageability, it was confirmed that all samples have a well consolidated porous structure with excellent structural integrity. Thus, they can be handled without collapsing or delaminating.

3.1. Microstructural characterization

The study of the porosity of the Taguchi sample series by Hg porosimetry experiments allowed assessing the three following output

Table 2
Structural properties of the sample series and Taguchi's output factors: good or bad manageability, porosity, typical pore size, existence of pores larger than 100 μm, and Young's modulus. Porosity was estimated assuming a skeleton of bulk alumina with ρ_{sk} = 3.985 g/cm^3.

Sample series	Manageability	Porosity (%)	Typical pore size (μm)	∃ Pores >100 μm?	Young's Modulus (GPa)
T1	Good	68.9	>200	Yes	1.1 ± 0.6
T2	Good	71.0	>250	Yes	1.6 ± 1.0
T3	Good	62.6	>250	Yes	1.7 ± 1.1
T4	Good	75.1	>250	Yes	3.3 ± 1.5
T5	Good	68.2	40	Yes	1.2 ± 0.9
T6	Good	76.6	>250	Yes	1.5 ± 0.4
T7	Good	75.3	>250	Yes	1.1 ± 0.6
T8	Good	80.9	240	Yes	1.6 ± 1.0

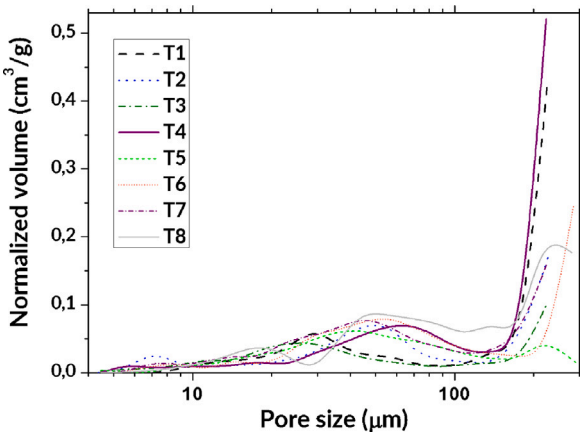

Fig. 2. Pore size distributions of the sample series obtained by Hg porosimetry.

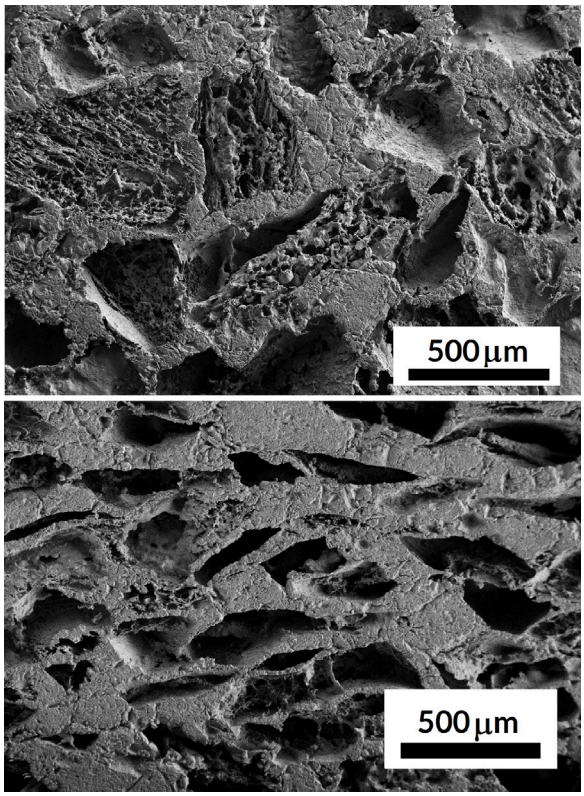

Fig. 3. SEM images of the typical pores observed in the porous constructs. Top: image from in-plane surface of sample T2; bottom: cross-section surface of sample T4, where the axis of the load during sintering is the vertical direction of the image.

factors of the Taguchi analysis: porosity, typical pore size, and the existence of pores with sizes above 100 μm. The influence of the initial amount of sacrificial carbon and the sintering temperature on the final porosity of the alumina porous samples can be seen in the data included in Table 2 (and in Figure SI.1, in the Supplementary Information). Clearly, a higher amount of carbon in the initial powder mixture implies a higher final porosity of the sample, as expected. In contrast, the expected effect of the temperature was not confirmed, and higher porosities were obtained for higher temperatures of the thermal treatment, on average.

It was verified that all the samples have high porosities, but, according to the "the larger is better" criterion, samples T4, T6, T7 and T8 are the most adequate. Nevertheless, the samples were fabricated with specific amounts of sacrificial carbon to achieve the target porosities of 40% and 50%. However, the obtained experimental porosities were found to lie between 62% and 80%, which turned out to be higher than the expected ones, probably because the complete densification of the alumina skeleton did not occur. Therefore, these high porosities may lead to an excessive decrease of the mechanical properties.

The pore size distributions of the samples are plotted in Fig. 2. All the samples exhibit a bimodal distribution where the majority population, except in T5, is found in pores larger than 200 μm, which is the target range. Therefore, the sample T5 was discarded because its population of pores has, mainly, a size of 40 μm and only exhibits very few pores with sizes above 200 μm. Finally, Hg porosimetry revealed that pores can also be found with sizes smaller than 100 μm in all samples. Considering this factor, the most remarkable sample among all the set is T4 because it is the one with the largest population of pores of more than 200 μm.

Further structural research using SEM confirmed that the eight samples have a similar morphology at the microscale. A selection of representative images is shown in Fig. 3. On the one hand, the top and center images of Fig. 3 correspond to the in-plane perspective (namely, the plane perpendicular to the applied load during sintering; see Ref. [38] for more details). It shows pores clearly larger than 100 μm. In this plane, the shape of the pores does not have a preferential feature. In contrast, bottom image, corresponding to the cross section (namely, a plane parallel to the applied load during sintering) show that the pores have an acicular shape and preferential orientation, which is perpendicular to the axis of the load applied during the sintering. In addition, small pores with sizes well below 100 μm can be also seen, demonstrating the bimodality in pore size that the Hg porosimetry distribution revealed. The average pore size is on the order of 200–400 μm. So, considering the microstructure observed by SEM imaging in these two perpendicular planes, the anisotropy imposed by the uniaxial load during sintering and the average features of the porosity revealed by Hg porosimetry can also be confirmed. Finally, detailed inspection of the images confirmed that highly porous alumina regions can be found randomly dispersed in a fully dense alumina skeleton, which can explain the good manageability of the samples at the macroscale and the high values of the porosity obtained.

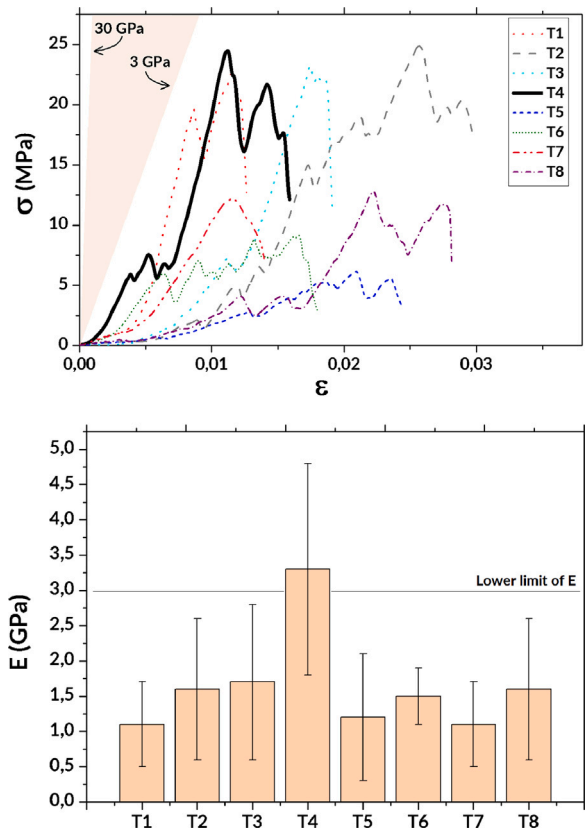

Fig. 4. Top: representative stress–strain curves of the sample series. The Young's modulus of each experiment was estimated as the average initial slope. The region where the stress–strain curves for the target Young's modulus values would be found has been colored in light brown for reference. Bottom: values of the Young's modulus of the eight fabricated samples. Uncertainties are taken as one standard deviation.

3.2. Mechanical properties

The mechanical properties of the samples were studied by uniaxial compression tests, focusing on the values of the Young's modulus. The stress–strain curves of these tests are shown in Fig. 4, top. This graph also shows the target region (in light brown) in which the theoretical stress–strain curves of cortical bone would be found. All the curves display the typical discontinuous behavior corresponding to porous irregular materials, exhibiting failures up to the maximum borne load and fracture. The obtained average values of the eight Young's moduli are given in Table 2 and Fig. 4, bottom. This analysis confirmed that all the samples have a modulus on the order of 1 GPa, except T4 (solid black line), which has 3.3 GPa, slightly above to the lower required mechanical threshold of 3 GPa [10]. It is worth noting that the residual carbon present in the porous structures may reduce their mechanical properties [18], so removing this carbon would yield a better mechanical performance.

According to the mechanical analysis, the fabrication procedure used for sample T4 is clearly the best procedure for obtaining candidates for cortical bone implant, among the tested procedures. However, although the structural requirements were fulfilled, its mechanical performance is still below that of cortical bone. Therefore, Taguchi's analysis must be performed in order to identify the most effective changes to be made in the fabrication procedure for the improvement of the porous alumina samples.

3.3. Discussion of the Taguchi analyses

As a first step, the correlation matrix between the input factors and all the quantitative output factors has been calculated. In Table 3, the correlation coefficients and the *p*-statistical power values are shown. For a significance $\alpha = 0.05$, all the *p*-coefficients meet the condition $p > \alpha$, therefore, all the correlation coefficients are significant. The strongest correlations (>0.5, highlighted in Table 3) confirm the paramount and evident influence of the carbon sacrificial template content (factor "A") with the porosity. Moreover, the consolidation temperature (factor "D") is revealed as other very relevant factor for the porosity and the Young's modulus.

In addition, as explained before, "the larger is better" criterion is employed throughout the analysis because the objective is to gather the coexistence of high porosity, large pore sizes (>100 μm) and high Young's modulus (3–30 GPa), along the qualitative features related to manageability and existence of pores larger than 100 μm. That is, it is sought that the values of all these magnitudes must be as high as possible at the same time, even though some of these magnitudes are inversely related, such as the mechanical properties and the porosity.

The set of results of the eight quasiexperiments (shown in Table 2) was analyzed through the Taguchi method, and the values of the S/N ratio of each factor at each level are shown in the answer Table 4. These values, if plotted, visually highlights the importance of each input: the steeper the slope, the greater its influence on the process (Figure SI.2). In addition, the highest average response characteristic value minus the lowest average response characteristic value for levels of that factor, namely, the δ factor, is also shown, along the ranking of influence for the factors. On the one hand, the appropriate level of each input factor will be the one with the highest S/N ratio. That is, the optimal combination of values of the parameters affecting the fabrication procedure is, precisely, that of the quasiexperiment T4. On the other hand, this analysis revealed that the two most influential factors in the porous alumina manufacturing process are the amount of carbon and the temperature of the final thermal consolidation treatment. That is, the two most important factors are the amount of sacrificial carbon (lower is preferable), a foreseeable result given the major role of the sacrificial template in the final porosity, and, interestingly, the temperature of the final consolidation heat treatment (higher is preferable). Finally, the estimated linear model coefficients for S/N are shown in Table SI.1, in the Supporting Information. This model, which has an R^2 explained variance of 0.992, confirmed that the only non-significant dependence (with an error type-II = 0.675) is that of the factor "E", the plateau time of the thermal treatment. Therefore, the lowest value of this parameter can be chosen for subsequent procedures to save energy and time.

Table 3
Correlation coefficients (and *p-statistical power values* below) of the quantitative output factors of the Taguchi analysis regarding the input factors: A, carbon content; B, SPS sintering plateau time; C, calcination heating rate; D, thermal consolidation treatment temperature; E, thermal consolidation treatment plateau time. The highest correlations are highlighted.

	A	B	C	D	E
Porosity	**0.541** *0.166*	0.213 *0.613*	−0.315 *0.448*	**0.662** *0.074*	0.140 *0.974*
Pore size	−0.310 *0.455*	0.456 *0.256*	−0.274 *0.512*	0.456 *0.256*	−0.274 *0.512*
Young's modulus	−0.431 *0.286*	0.431 *0.286*	0.431 *0.286*	**0.544** *0.164*	0.244 *0.561*

Table 4
Answer table for the S/N ratio, the δ factor, and the ranking of influence for the factors: A, carbon content; B, SPS sintering plateau time; C, calcination heating rate; D, thermal consolidation treatment temperature; E, thermal consolidation treatment plateau time.

Level	A	B	C	D	E
1	8.509	7.304	7.360	7.053	7.832
2	7.233	8.438	8.381	8.689	7.910
δ	1.276	1.134	1.021	1.637	0.078
Ranking	2	3	4	1	5

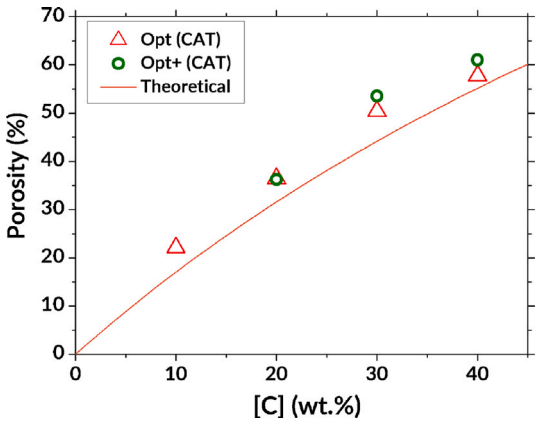

Fig. 5. Total porosities and typical pore sizes for different nominal carbon contents. Solid line indicates the expected theoretical porosity in dependence on the carbon content, assuming a skeleton of bulk alumina with ρ_{sk} = 3.985 g/cm^3 and carbon sacrificial phase with ρ_{carbon} = 2.1 g/cm^3).

The last analysis consisted of a test of non-linearity including second-order interaction terms. Interestingly, the only significant second-order interaction was found between the two time-related factors, namely, factor "B", plateau for SPS plateau time, and "C", thermal treatment plateau time. Both lines not only are not parallel, but they intersect, indicating crossed correlation.

3.4. Optimization of the fabrication procedure according to the Taguchi analyses

3.4.1. Optimized fabrication conditions

A new study has been conducted in which the fabrication procedure was varied according to the conclusions of the previous Taguchi analysis. The two more influential factors of the procedure were researched: carbon content and the temperature of the final thermal treatment. The considered carbon contents were 10, 20, 30, and 40 wt%. On the other hand, the temperature of the final thermal treatment was kept at 1400 °C (2 h) for sample series "Opt", and increased at 1600 °C (2 h) for sample series "Opt+". The rest of the preparation conditions remain the same as quasiexperiment T4. The samples were labeled as "Opt*X*" and "Opt+*X*", where *X* indicates the weight percentage of carbon. The objective is to determine the minimum quantity of carbon that can be used in the initial mixture, and the effect of the temperature of the final thermal consolidation treatment, while always fulfilling the simultaneous presence of adequate porosity and mechanical properties. Note that the carbon sacrificial content should be reduced but should be high enough to ensure interconnected porosity.

The first effect of the optimized processes concerns the optical aspect of the samples and the presence of stains, as the content of impurities is reduced with the strongest thermal treatment of Opt+ procedure. XRF analyses of the sample series containing 40 wt% of carbon, namely, T4, Opt40, and Opt+40 revealed that the final consolidation thermal treatment is beneficial for the elimination of residual carbon and Fe-related reddish stains. The traces of Fe in the samples are significantly reduced from 0.64 wt% in the case of the sample with the mildest thermal treatment, Opt40 (2 h at 1400 °C), to 0.49 wt% in sample T4 (4 h at 1400 °C) and 0.27 wt% for sample Opt+40, consolidated with the strongest thermal treatment (2 h at 1600 °C). The whiteness and the reduction of the Fe-containing stains can be assessed in the optical images shown in Figure SI.3, in the Supporting Information.

3.4.2. Structural properties of the optimized series

These optimized sample series were submitted to structural characterizations through CAT and SEM. In these samples, the study of the porous space was made by CAT, which allows the estimation of pore interconnectivity, instead of Hg porosimetry. The most relevant structural parameters and the dependence of the porosity with the carbon content can be seen in Table 5 and in Fig. 5, respectively. In the Opt and Opt+ series, the monotonic increasing relationship between the carbon content and the porosity can be constated, as expected. Note that these results are close to the expected theoretical data (solid line), obtained from the respective densities of the starting phases, alumina and carbon powder, supporting the accuracy of this new optimized method. The experimental values are slightly higher than the expected theoretical values (+15% higher in average) probably because the alumina skeleton is not fully densified and some small porosity still remains. In addition, both sets of samples have similar porosities for the same amount of carbon. This indicates that final heat treatment at a higher temperature does not affect the overall porosity.

SEM images (Fig. 6) revealed the already known anisotropy due to the uniaxial pressure applied during sintering, and a preferred orientation of the pores in the perpendicular plane to the axis of pressure can be clearly seen. An important difference between the Opt and Opt+ sample series concerns the presence of regions with microsized pores: while samples Opt exhibit pores in the range of a few microns (at magnification x100 they look like wrinkled regions, e.g. Fig. 6, top), similarly to samples from the previous Taguchi analysis (Fig. 3), the higher heat treatment applied to samples Opt+ extinguishes, or densifies, these regions with small pores, and only large pores formed by the thick skeleton remain (Fig. 6, bottom). In addition, the very frequent existence of pores of sizes above 200 μm was also confirmed. It is worth remarking that the existence of pores with sizes beyond 200 μm as a significant structural feature means that this kind of samples exhibits ideal pore sizes for cell proliferation in case they may be considered as an alternative for the development of materials for cortical bone tissue engineering [9,42].

Special attention should be paid to the CAT analyses of these sample series as this technique provided images such as those shown in Fig. 7, in which it can be confirmed that the porous structure observed in surface from SEM is representative of the whole bulk of the samples. In addition, the 2.72 μm resolution gives an accurate spatial disposition of the porous space (blue regions in Fig. 7, bottom). Hence, the interconnectivity of the porous space could be assessed, giving rise to the values indicated in Table 5. Thus, samples with 30 wt% of carbon or more exhibit a very high degree of interconnectivity, above 90%. This is a very significant structural feature for possible cortical bone tissue engineering applications since large pores between 150–500 μm with interconnectivity above 60% are ideal for osteoinduction [43].

3.4.3. Mechanical properties of the Optimized series

The uniaxial compression tests performed on these new sample series gave the stress–strain curves plotted in Fig. 8, top, and the corresponding Young's moduli and compression strengths are shown in Fig. 8, bottom, and in Table 5. Firstly, comparing the behavior of Opt and Opt+ series with those of the previous samples (Fig. 4), a significant increase of the mechanical performance is clearly found, confirming the appropriateness of the conclusions of the Taguchi's analysis. In addition, the increase of the Young's moduli with decreasing carbon content is apparent, and the aimed lowest value of the Young's modulus is achieved, and even surpassed, for all the carbon contents. In other words, all the obtained samples emulate the mechanical elastic performance of the human cortical bone since their Young's moduli are within the limits of the theoretical Young's modulus of the cortical bone (3–30 GPa [10], boundaries of the light brown zone in Fig. 8, top). In addition, the values of the compression strength of the sample series are all above the typical values of the load supported by bones during daily activities, which has bee established in 4 MPa [44]. Therefore,

Table 5
Structural and mechanical properties of the optimized sample series. Porosity was estimated assuming a skeleton of bulk alumina with $\rho_{sk} = 3.985$ g/cm^3. Sample Opt+10 was discarded given the very low porosity of the sample Opt10.

Sample series	Porosity by CAT (%)	Pore interconnectivity (%)	Young's modulus (GPa)	Compression strength (MPa)
Opt10	22.1	7.9	9.2 ± 1.4	158 ± 46
Opt20	36.4	60.0	7.4 ± 1.4	86 ± 22
Opt30	50.4	96.4	5.6 ± 1.2	52 ± 20
Opt40	57.7	98.8	3.6 ± 1.1	25 ± 11
Opt+10	–	–	14.2 ± 2.7	184 ± 66
Opt+20	36.2	36.9	6.9 ± 1.8	83 ± 38
Opt+30	53.5	96.5	5.5 ± 1.1	49 ± 20
Opt+40	61.0	98.3	3.2 ± 0.8	25.1 ± 8.3

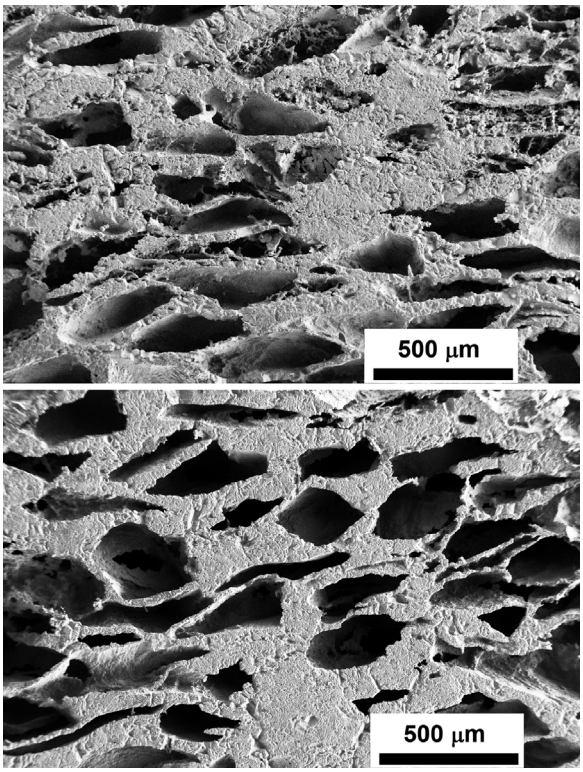

Fig. 6. SEM images of cross-section surfaces of samples Opt30 (top) and Opt+30 (bottom). The axis of the load during sintering is the vertical direction of the images.

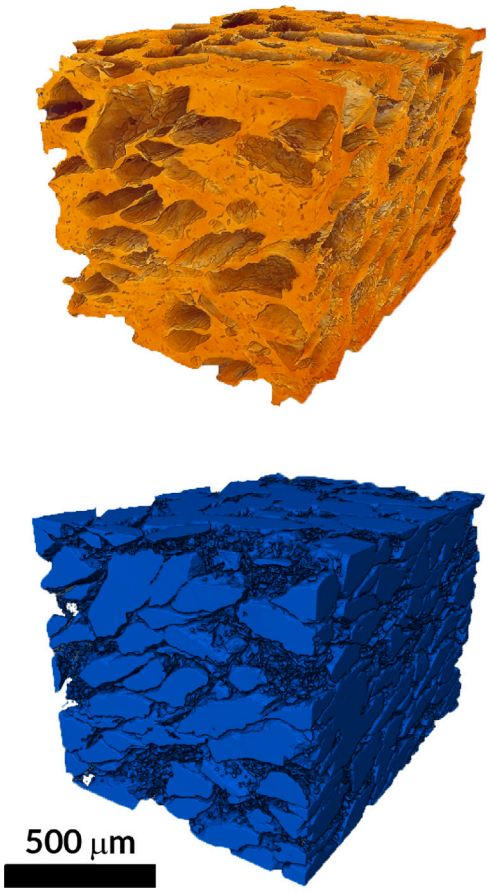

Fig. 7. CAT representations of the alumina skeleton of sample Opt+30 (top), and its complementary porous space (bottom). Scale bar corresponds to both images. (For interpretation of the references to color in this figure legend, the reader is referred to the web version of this article.)

the mechanical behavior of both Opt and Opt+ is similar, meaning that the higher thermal treatment of sample Opt+ has no influence on the mechanical properties of these structures. Finally, the obtained values of the Young's moduli are significantly lower than the expected values from the models of porous alumina [30], which can be found in the range of 50–250 GPa, confirming that the strengthening of the skeleton can be even further enhanced.

4. Conclusions

This research introduces an original fabrication procedure of porous alumina constructs based on carbon sacrificial template and reactive spark plasma sintering. The procedure was optimized according to the challenge of fabricating alumina samples that emulate the subtle combination of the physical properties of the human cortical bone, such as porosity (porous sizes and interconnectivity), and the mechanical properties (Young's modulus and strength). The design of the procedure was performed through the Taguchi analysis, which revealed that the sacrificial template content and the temperature of the final consolidation heat treatment were most influential factors concerning the aimed at physical properties. Thus, the fabrication process was modified according to the conclusions of Taguchi analysis, and optimized samples that accomplish the required combination of physical properties, were obtained. Hence, optimized samples with carbon contents above 10 wt% exhibited high porosity values (>36%), with most of the pores larger than 200 μm, a highly interconnected pore structure (>60%), and Young's modulus higher than 3 GPa and strength higher than 4 MPa, the characteristic minimum values of the mechanical properties of the human cortical bone. In summary, the results confirmed this optimized procedure to be an innovative route for the fabrication of porous alumina constructs mimicking the physical properties of the cortical bone, which may make them appropriate for bioactivation procedures and future applications in bone tissue engineering.

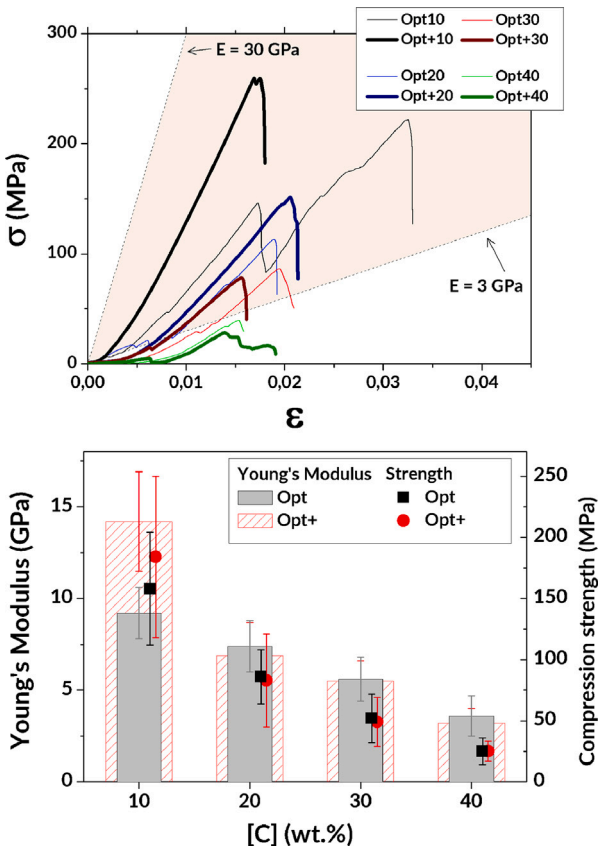

Fig. 8. Top: stress–strain curves of the optimized sample series Opt (thin lines) and Opt+ (thick lines). Numbers of the labels in the legend indicate the carbon content, [C], in wt.%. The limits of the Young's modulus of the human cortical bone (3–30 GPa) are indicated by the light brown triangular region. Bottom: dependence of the mechanical properties of the sample series on the carbon content. Compression strength data were slightly laterally shifted for clarity.

CRediT authorship contribution statement

Manuela González-Sánchez: Conceptualization, Formal analysis, Data curation, Investigation, Validation, Writing – original draft, Writing – review & editing. **Pedro Rivero-Antúnez:** Data curation, Investigation, Validation, Writing – review & editing. **Francisco Luis Cumbrera-Hernández:** Conceptualization, Formal analysis, Data curation, Validation, Writing – review & editing. **Víctor Morales-Flórez:** Conceptualization, Formal analysis, Writing – review & editing, Funding acquisition, Supervision.

Declaration of competing interest

The authors declare that they have no known competing financial interests or personal relationships that could have appeared to influence the work reported in this paper.

Acknowledgments

Project PGC2018-094952-B-I00 funded by *FEDER and Ministerio de Ciencia e Innovación* - Agencia Estatal de Investigación, Spain, Project P20-01121 (FRAC) funded by Junta de Andalucía, Spain (Consejería de Transformación económica, Industria, Conocimiento y Universidades) and Project 2023/00000372 from the VII Plan propio de investigación de la Universidad de Sevilla, Spain, are acknowledged. The FQM-163 research group is deeply acknowledged for its help with the mechanical characterization of the samples. Prof. Camilo Zamora-Ledezma from (UCAM, Spain) is acknowledged for his ideas and wise suggestions. All the members of the FQM393 research group are greatly acknowledged for their support.

Appendix A. Supplementary data

Supplementary material related to this article can be found online at https://doi.org/10.1016/j.jmrt.2024.02.099.

References

[1] Mackay S. Materials: engineering, science, processing and design. vol. 164, 2011, http://dx.doi.org/10.1680/coma.1000013.
[2] Morales-Flórez V, Domínguez-Rodríguez A. Mechanical properties of ceramics reinforced with allotropic forms of carbon. Prog Mater Sci 2022;128:100966.
[3] Suleiman B, Zhang H, Ding Y, Li Y. Microstructure and mechanical properties of cold sintered porous alumina ceramics. Ceram Int 2022;48(10):13531–40.
[4] Park J. In: York SN, editor. Bioceramics: properties, preparation and applications. 1st ed.. New York: Springer; 2008.
[5] Ruys A. 1 - introduction to alumina ceramics. In: Ruys A, editor. Alumina ceramics. Woodhead publishing series in biomaterials, Woodhead Publishing; 2019, p. 1–37. http://dx.doi.org/10.1016/B978-0-08-102442-3.00001-4.
[6] Ali MS, Azmah Hanim MA, Tahir SM, Jaafar CN, Norkhairunnisa M, Matori KA. Preparation and characterization of porous alumina ceramics using different pore agents. J Ceram Soc Japan 2017;125(5):402–12.
[7] Salvini VR, Pandolfelli VC, Spinelli D. Mechanical properties of porous ceramics. In: Al-Naib UMB, editor. Recent advances in porous ceramics. Rijeka: IntechOpen; 2018, http://dx.doi.org/10.5772/intechopen.71612.
[8] Yang S. The design of scaffolds for use in tissue engineering. Part i. traditional factors. Tissue Eng 2001;7(6):679–89.
[9] Ebnesajjad S. In: Ebnesajjad S, editor. Handbook of biopolymers and biodegradable plastics. properties, processing and applications. 1st ed.. Elsevier; 2012.
[10] Jia Z, Xu X, Zhu D, Zheng Y. Design, printing, and engineering of regenerative biomaterials for personalized bone healthcare. Prog Mater Sci 2023;134(April 2021):101072.
[11] Krafts KP. In: Li X, editor. Tissue repair. reinforced scaffolds. 1st ed.. Singapure: Springer Nature Singapore; 2017, p. VII, 304. http://dx.doi.org/10.1007/978-981-10-3554-8.
[12] Stanciuc AM, Sprecher CM, Adrien J, Roiban LI, Alini M, Gremillard L, Peroglio M. Robocast zirconia-toughened alumina scaffolds: Processing, structural characterisation and interaction with human primary osteoblasts. J Eur Ceram Soc 2018;38(3):845–53.
[13] Roleček J, Pejchalová L, Martínez-Vázquez FJ, Miranda González P, Salamon D. Bioceramic scaffolds fabrication: Indirect 3D printing combined with ice-templating vs. robocasting. J Eur Ceram Soc 2019;39(4):1595–602.
[14] Paredes C, Martínez-Vázquez FJ, Pajares A, Miranda P. Novel strategy for toughening robocast bioceramic scaffolds using polymeric cores. Ceram Int 2019;45(15):19572–6.
[15] López-González I, Zamora-Ledezma C, Sanchez-Lorencio MI, Barrenechea ET, Gabaldón-Hernández JA, Meseguer-Olmo L. Modifications in gene expression in the process of osteoblastic differentiation of multipotent bone marrow-derived human mesenchymal stem cells induced by a novel osteoinductive porous medical-grade 3d-printed poly(ϵ-caprolactone)/β-tricalcium phosphate c. Int J Mol Sci 2021;22(20):1–21.
[16] Paredes C, Martínez-Vázquez FJ, Pajares A, Miranda P. Co-continuous calcium phosphate/polycaprolactone composite bone scaffolds fabricated by digital light processing and polymer melt suction. Ceram Int 2021;47(12):17726–35.
[17] Garot C, Bettega G, Picart C. Additive manufacturing of material scaffolds for bone regeneration: Toward application in the clinics. Adv Funct Mater 2021;31(5):2006967.
[18] Paredes C, Roleček J, Pejchalová L, Miranda P, Salamon D. Impact of residual carbon after DLP and SPS-sintering on compressive strength and in-VITRO bioactivity of calcium phosphate scaffolds. Open Ceram 2022;11(June).
[19] Toledo-Fernández JA, Mendoza-Serna R, Morales V, De La Rosa-Fox N, Piñero M, Santos A, Esquivias L. Bioactivity of wollastonite/aerogels composites obtained from a TEOS-MTES matrix. J Mater Sci: Mater Med 2008;19(5):2207–13.
[20] Almeida JC, Wacha A, Gomes PS, Alves LC, Fernandes MHV, Salvado IM, Fernandes MHR. A biocompatible hybrid material with simultaneous calcium and strontium release capability for bone tissue repair. Mater Sci Eng C 2016;62:429–38.
[21] González-Sánchez M, Morales-Flórez V, Rivero-Antúnez P, Esquivias Fedriani L, Reyes Peces M. Bioactivación de la alúmina mediante el uso de silicatos de calcio y disolución piraña. 2023, Spanish patent application, n° P202330214.
[22] Hooshmand S, Nordin J, Akhtar F. Porous alumina ceramics by gel casting: Effect of type of sacrificial template on the properties. Int J Ceram Eng Sci 2019;1(2):77–84.

[23] Dele-Afolabi T, Azmah-Hanim M, Norkhairunnisa M, Sobri S, Calin R, Ismarrubie Z. Significant effect of rice husk and sugarcane bagasse pore formers on the microstructure and mechanical properties of porous al2o3/Ni composites. J Alloys Compd 2018;743:323–31.
[24] Rizwan A, Anwar M, Kim J, Song I, Abbas S, Ali S, Ali F, Ahmad J, Awais H, Mehmood M. Porosity features and gas permeability analysis of bi-modal porous alumina and mullite for filtration applications. Ceram Int 2016;42:18711–7.
[25] Claro A, Alves C, Dos Santos K, Da Rocha E, Fontes M, Monteiro G, Gonçalves de Carvalho G, Caiut J, Moroz A, Ribeiro S, Barud H. Regenerated cellulose sponge as sacrificial template for the synthesis of three-dimensional porous alumina-silica scaffold for tissue engineering. J Sol-Gel Sci Technol 2023;107:83–95.
[26] Choi DH, Kamada K, Enomoto N, Hojo J, Lee SW. Fabrication of porous alumina ceramics by spark plasma sintering method. Adv Mater Res 2007;24–25:279–82.
[27] Cho WS, Yoo YC, Whang CM, Cho NH, Kim JG, Kwon YJ, Munir ZA. Preparation of porous alumina ceramics by spark plasma sintering. Key Eng Mater 2007;336–338:1056–9.
[28] Pascual Rodríguez Y, Rivero-Antúnez P, Morales-Flórez V. Material cerámico poroso y su obtención mediante el método de plantillas sacrificables para su uso como andamios tisulares. 2020, P202030913, Spanish patent, n° ES2898685.
[29] Wang X, Chen C, Wang Y. Fractal analysis of porous alumina and its relationships with the pore structure and mechanical properties. Fractal Fract 2022;6(8):460.
[30] González-Sánchez M, Rivero-Antúnez P, Cano-Crespo R, Morales-Flórez V. Fabrication of porous alumina structures by SPS and carbon sacrificial template for bone regeneration. Materials 2022;15(5):1754.
[31] Beyer HG, Sendhoff B. Robust optimization - a comprehensive survey. Comput Methods Appl Mech Engrg 2007;196(33–34):3190–218.
[32] Logothetis N, Wynn HP. Quality through design: experimental design, off-line quality control and Taguchi's contributions. Oxford series on advanced manufacturing 7, Oxford: Clarendon Press; 1994.
[33] Medina PD, Cruz EA, Restrepo JH. Aplicación del modelo de experimentacion Taguchi en un ingenio azucarero del valle del cauca. Scientia 2007;XIII(34):337–41.
[34] Rao RS, Kumar CG, Prakasham RS, Hobbs PJ. The Taguchi methodology as a statistical tool for biotechnological applications: A critical appraisal. Biotechnol J 2008;3(4):510–23.
[35] Ebrahimi M, Mobasherpour I, Bafrooei HB, Bidabadi FS, Mansoorianfar M, Orooji Y, Khataee A, Mei C, Salahi E, Ebadzadeh T. Taguchi design for optimization of structural and mechanical properties of hydroxyapatite-alumina-titanium nanocomposite. Ceram Int 2019;45(8):10097–105.
[36] Ajaal TT, Smith RW. Employing the Taguchi method in optimizing the scaffold production process for artificial bone grafts. J Mater Process Technol 2009;209(3):1521–32.
[37] Bhargav A, Min KS, Wen Feng L, Fuh JYH, Rosa V. Taguchi's methods to optimize the properties and bioactivity of 3D printed polycaprolactone/mineral trioxide aggregate scaffold: Theoretical predictions and experimental validation. J Biomed Mater Res - B 2020;108(3):629–37.
[38] Rivero-Antúnez P, Cano-Crespo R, Sánchez-Bajo F, Domínguez-Rodríguez A, Morales-Flórez V. Reactive SPS for sol–gel alumina samples: Structure, sintering behavior, and mechanical properties. J Eur Ceram Soc 2021;41(11):5548–57.
[39] Kumagai M, Messing GL. Enhanced densification of boehmite sol-gels by α-alumina seeding. J Am Ceram Soc 1984;67(11):c230–1.
[40] Caeiro J, González P, Guede D. Biomecánica y hueso (y II): ensayos en los distintos niveles jerárquicos del hueso y técnicas alternativas para la determinación de la resistencia ósea. Rev Osteoporos Metab Miner 2013;5(2):99–108.
[41] Marco Martinez F, Urda Martinez-Aedo AL. In: Marco Martinez F, Urda Martinez-Aedo AL, editors. Traumatologia y ortopedia para el grado en medicina. Barcelona: Elsevier; 2015.
[42] Vallet-Regí M, Ruiz-Hernández E. Bioceramics: From bone regeneration to cancer nanomedicine. Adv Mater 2011;23(44):5177–218.
[43] Liu F, Huang B, Hinduja S, Silva Bartolo PJ. Biofabrication techniques for ceramics and composite bone scaffolds. In: Bioceramics and biocomposites. 2019, p. 17–37. http://dx.doi.org/10.1002/9781119372097.ch2.
[44] Dorozhkin SV. Calcium orthophosphate ($CaPO_4$)-based bioceramics: Preparation, properties, and applications. Coatings 2022;12(10):1380.